



## Research article

# Bifunctional folic acid targeted biopolymer Ag@NMOF nanocomposite [ $\{Zn_2(1,4\text{-}bdc)_2(DABCO)\}_n$ ] as a novel theranostic agent for molecular imaging of colon cancer by SERS

Fatemeh Mahboubi<sup>a</sup>, Javad Mohammadnejad<sup>b</sup>, Sepideh Khaleghi<sup>a,\*</sup><sup>a</sup> Department of Biotechnology, Faculty of Advanced Science and Technology, Tehran Medical Sciences, Islamic Azad University, Tehran, Iran<sup>b</sup> Department of Life Science Engineering, Faculty of New Sciences and Technologies, University of Tehran, Tehran, Iran

## ARTICLE INFO

## Keywords:

Green synthesis  
Silver nanoparticles  
Chitosan-folic acid nanoparticles  
NMOF  
Theranostic agent  
Colon cancer  
Molecular imaging  
SERS

## ABSTRACT

Without a doubt, cancer and its negative impact on human health have created many hurdles for people across the world since conventional approaches have not offered a reliable ability in the eradication of cancer. As a result, finding novel approaches, like using bimodal nanoparticles as a potential nanocarrier in molecular imaging and cancer therapy, is remarkably required these days. In the present study, ex-situ (Ge) and in-situ (Gi) green synthesized silver (Ag) nanoparticles entrapped in metal-organic framework nanocomposites (NMOF) coated with folic acid (FA) targeted chitosan (CS) was successfully developed as a novel bifunctional nanocarrier for detection and treatment of colon cancer cells. Then nanocarriers, such as NMOF-CS-FA, Ge-Ag@NMOF-CS-FA, Gi-Ag@NMOF-CS-FA, and C-Ag@NMOF-CS-FA, were characterized via FT-IR, DLS, SERS, TEM, and SEM and results have potentially confirmed the quality and quantity of synthesized nanocomposites. The hydrodynamic diameters of NMOF-CS, Ge-Ag@NMOF-CS, Gi-Ag@NMOF-CS, and C-Ag@NMOF-CS specimens were measured at around  $99.7 \pm 10$  nm,  $110 \pm 10$  nm,  $118 \pm 10$  nm,  $115 \pm 10$  nm, respectively. Also, the PDI values less than 0.2 confirm the reliable distribution of these nanocomposites. Afterward, the cell viability assay was conducted on HCT116 and HGF cell lines for evaluating biocompatibility and targeting efficiency of nanocomposites; FA functionalized nanocomposites have intensively indicated better performance in cancer cells targeting and their inhibition, and IC50 was attained for 10 ng/mL of Ge-Ag@NMOF-CS-FA while non-targeted nanocarriers did not have toxicity more than 20 % on HCT116 colon cancer cells. Moreover, according to the results, the cell viability of HGF normal cells was at least 85 % after being exposed to different concentrations of nanocomposites for 24 h. This indicates that the synthesized nanocomposites do not have significant toxic effects on normal cells. The results indicate that this novel nanocomposite has the potential to effectively deliver drugs to cancer cells.

## 1. Introduction

Cancer, as one of the most serious health problems worldwide, is among the top reasons for death [1]. The total number of patients

\* Corresponding author. Medical Biotechnology, Faculty of Advanced Science and Technology, Tehran Medical Sciences, Islamic Azad University, Tehran, Iran.

E-mail address: [s.khaleghi@iautmu.ac.ir](mailto:s.khaleghi@iautmu.ac.ir) (S. Khaleghi).

<https://doi.org/10.1016/j.heliyon.2024.e29876>

Received 20 November 2023; Received in revised form 16 April 2024; Accepted 16 April 2024

Available online 18 April 2024

2405-8440/© 2024 The Authors. Published by Elsevier Ltd. This is an open access article under the CC BY-NC license (<http://creativecommons.org/licenses/by-nc/4.0/>).

with cancer per year is predicted to considerably increase and reach relatively 12 million by 2030 across the world [2]. Colon cancer ranks third among the most frequently occurring cancers and fourth among the most lethal cancers across the world [3]. Annually, more than 500,000 deaths are recorded for patients with colorectal cancer across the globe which is an eye-catching value [4]. Furthermore, despite attempts to suppress cancer, its treatment remarkably encountered various challenges; therefore, finding a practical approach to early diagnosis and detection of cancer will considerably increase the survival rate of most cancer patients [5]. On the other hand, conventional cancer diagnosis approaches including X-ray computed tomography (CT), magnetic resonance imaging (MRI), biopsy, and so forth have not satisfied patients with cancer and physicians due to lack of specificity, low specificity, inability to target cancer sites, less sensitivity, considerable side effects, etc. [5,6]. As a result, novel approaches are rising, like nanoscale “Trojan horses” with the aim of delivering diagnostics to the exact sites of cancer cells [7]. Among various approaches, surface-enhanced Raman scattering spectroscopy (SERS) has attracted the attention of physicians as a practical and easy-to-use device in bioimaging fields because of its specific aspects such as photostability, incomparable virtues of very high sensitivity, narrow fingerprint signature, etc. Compared to the conventional fluorescence approaches [8].

Bifunctional nanoparticles-based systems have been considered a promising approach in the diagnosis and therapy of cancer (Theranostic) and are creating a new window for effective suppression and detection of cancer by avoiding drug elimination from the small intestine, getting away from the immune system, decreasing the pre-systemic metabolism, enhancing stability and biocompatibility of therapeutics, increasing drug accumulation in cancer tissues, and so on which pave the way for improving the performance of therapeutics and cancer therapy [9–12]. Among various Trojan horses-like drug delivery devices, nanoscale Metal-Organic Frameworks (NMOFs) are highly effective in delivering therapeutics to cancer sites [13]. These vehicles are composed of self-assembled metal ions and organic linkers, and a combination of organic and inorganic elements has led to the emergence of some new properties, including biocompatibility, biodistribution, high drug loadings, biostability, etc., in these nanocarriers [14,15]. Different bonding forces between metal ions and tunable organic linker clusters have strengthened the integrity of the NMOF structure, making it stable in human body serum [16]. NMOFs are of greater importance in the delivery of theranostics due to their specific aspects including large accessible surface area, high efficiency in trapping drugs, a sustained release of drugs, and good porosity, which further delight their potential ability in cancer therapy [17]. Among metal ions embedded in NMOFs, silver (Ag) nanoparticles can serve as an effective diagnostic and therapeutic element against cancer cells; however, these nanoparticles have been mainly applied as an antibacterial agent rather than anticancer therapeutics [18]. Ag nanoparticles’ anticancer performance could be achieved by inducing oxidative stress (ROS) and inflammation, DNA damage, and dysfunctionality in mitochondria [19]. Ag nanoparticles can be biosynthesized according to green chemistry concepts which are better than chemical synthesis since using the biosynthesis approach could eliminate drawbacks of the chemical method, including negative environmental effects, expensiveness, high energy consumption, toxicity, and lack of stability [20,21]. Various research studies have explored the potential of utilizing *Spirulina* Cyanobacterium for biosynthesizing silver nanoparticles [22]. *Spirulina*’s diverse components make it an ideal candidate for this process, as they perform as reducing, stabilizing, and capping agents. Moreover, the Cyanobacterial compounds found in *Spirulina* have been found to effectively contribute to the reduction and stabilization of nano-sized particles [23]. The hydroxyl groups present in diethanolamine, a type of amine found in *Spirulina*, function as reducing agents [24–26]. Moreover, studies have shown that the proteins extracted from *Spirulina* serve as the primary capping agent, further reinforcing the involvement of these polysaccharides in the synthesis of Ag-NPs. The green synthesis of silver nanoparticles using *Spirulina* is a straightforward, environmentally benign, and safe method [27].

On the other hand, utilizing a mixture of different nanoparticles can remarkably increase the advantages of nano-delivery systems in cancer detection and therapy [28]. Chitosan (CS), as a promising biopolymer, is the most abundant, biocompatible, and biodegradable polysaccharide in nature which is contemplated as an appropriate nanocarrier for delivery of theranostics [29]. Excellent aspects of CS, including good solubility, non-immunogenicity, great bioavailability and stability, cost-effectiveness, suitable hydrophilicity, and good pharmacodynamics and pharmacokinetics, have made it an effective candidate for cancer diagnosis and therapy [30]. Besides, because of possessing primary amino and hydroxyl groups on the CS nanoparticle’s surface, the ability to carry a large amount of drug and gradually release it over time, and many other prominent characteristics, CS nanoparticles have been considered an appropriate material in combination with NMOFs [31]. To increase the internalization efficiency of nanocomposites, diverse ligands can be conjugated on the surface of nanocarriers, biomolecules like DNA/RNA aptamer, antibodies, folic acid, etc. are good examples of these ligands which can be attached to their receptors on the target cancer cells and actively internalize into cells which called active theranostics delivery systems [32,33]. Folic acid (FA) is a type of targeting agent that can bind to its receptor, which is presented on cancer cells’ surface. While the folic acid receptor is overexpressed on the membrane of different cancer cells, including breast, lung and colon cancer cells, it has a limited expression in normal cells. Therefore, the efficient uptake of nanocomposite in target cells can be facilitated by using folic acid [34,35].

Overall, colon cancer ranks third in the most common cancers across the world. One of the primary reasons that colon cancer can be life-threatening is that it is often diagnosed at a late stage. Conventional imaging techniques cannot fully detect all malignant tissues, so new diagnostic tools are needed. Nanoparticles, specifically those made of noble metals such as silver, can be used in surface-enhanced Raman spectroscopy (SERS), a precise method of molecular identification that is non-invasive, highly sensitive, and specific. Metal-organic frameworks (MOFs) can be used to increase the stability of silver nanoparticles. By synthesizing targeted biocompatible nanocomposites, SERS acts as an accurate and non-destructive method for early detection of cancer.

In the present study, Ag nanoparticles were synthesized based on the green synthesis concept. Then, CS nanoparticles were decorated with FA and coated on the synthesized Ag-NMOF nanocomposites. The effectiveness of Ag-NMOF nanocomposites was evaluated using different analytical techniques such as FT-IR, SERS, XRD, DLS, TEM and SEM. Moreover, the cell viability biomedical assay was carried out to determine their potential for suppressing colon cancer.

## 2. Material and methods

### 2.1. Materials and devices

CS (Mw: 50000–190000 Da), AgNO<sub>3</sub>, Folic acid (>95 %), 1-(3-dimethyl aminopropyl)-3-ethyl carbodiimide hydrochloride (EDC), N-hydroxysuccinimide sodium salt (NHS), zinc acetate dihydrate (Zn(OAc)<sub>2</sub> · 2H<sub>2</sub>O), tris-acetate-ethylenediaminetetraacetic acid (EDTA), di-methyl-sulphoxide (DMSO), sodium tripolyphosphate (TPP), MTT (3-(4, 5-Dimethyl thiazol-2-yl)-2,5-diphenyl tetrazolium bromide) salt, Terephthalic acid salt bought from Sigma Aldrich, Acetic acid bought from Merck, 96 % alcohol, DABCO ligand bought from Sigma Aldrich, Dimethylformamide (DMF) solvent bought from Merck, Sodium dodecyl sulfonate (SDS) bought from Sigma Aldrich, DMEM culture medium, Trypsin, Trypan Blue, PBS buffer, Penicillin-Streptomycin (Pen-Strep), fetal bovine serum (FBS). *Spirulina platensis* strain PCC 9108 was obtained from France. Roswell Park Memorial Institute (RPMI) 1640 medium was prepared from Gibco, UK. The HCT116 colon cancer cell and HGF normal cell lines.

The experiment employed various instruments for spectroscopic analyses including a PerkinElmer 843 Fourier transform infrared (FT-IR) spectrometer, and a D8-advance X-ray diffraction (XRD) machine from Bruker AXS, Germany. Surface Enhanced Raman Spectroscopy (SERS) analysis was conducted using LabRAM Aramis and Horiba Jobin Yvon. Dynamic light scattering (DLS) tests were carried out using NanoBrook 90 Plus from Brookhaven, USA. Transmission electron microscopy (TEM) images were acquired with a Philips EM 208S from the Netherlands.

### 2.2. Green synthesis of Ag nanoparticle

The green synthesis approach was utilized for the synthesis of Ag nanoparticles. For this purpose, ethanol was used as a solvent to extract spirulina extract. Ethanol has been widely used as a suitable solvent for the extraction of spirulina extract. Ethanol's enhanced solubility for a wide range of organic compounds enables more efficient extraction of bioactive molecules from Spirulina, compared to water-based methods. Ethanol's compatibility with organic compounds also preserves the bioactivity of extracted compounds, and its volatile nature allows for easy solvent removal, facilitating downstream applications. In practice, 30 g of *Spirulina platensis* powder was mixed with ethanol in an Erlenmeyer flask and stirred at room temperature for 15 min. The mixture was then filtered with Whatman paper No. 1 after centrifugation at 4000 rpm for 30 min. Following this, 1 mM AgNO<sub>3</sub> solution was prepared by adding AgNO<sub>3</sub> to the filtrate and incubated overnight at room temperature, which was followed by yielding a brown solution that confirmed the successful formation of silver nanoparticles. The mixture was purified through centrifugation at 12,000 rpm for 16 min, the pellet was washed three times utilizing deionized water, dispersed in deionized water, and used for physical and chemical characterization.

### 2.3. Synthesis of CS-FA nanocomposite

The folic acid was activated using EDC and NHS salts as the following approach. The process of bioconjugation involves the activation of folic acid (FA) by EDC and NHS salts. EDC-NHS chemistry is utilized to bioconjugate ligands. EDC activates the carboxyl group of folic acid, making it more reactive, while NHS stabilizes the intermediate formed during the reaction [36]. 50 mg EDC and NHS were solubilized in 10 mL of DMSO and stirred for 2 h at room temperature and dark conditions. Afterward, folic acid weighing 280 mg was dissolved in a mixture containing EDC and NHS under stirring at 60 rpm in dark conditions and a nitrogen atmosphere at room temperature. Thereafter, 50 mg CS powder was suspended in 10 mL acetic acid (1 % v/w) and stirred at 70 rpm for 2 h. The mixture was then added to the activated folic acid mixture and stirred at 50 rpm in dark conditions for 24 h. Consequently, the solution containing CS was supplemented with 1 mM of NaOH. Then, the mixture was subjected to centrifugation at a speed of 4000 rpm for a duration of 15 min. Finally, the resulting precipitate was dried and preserved for conducting analytical and biomedical experiments.

### 2.4. Synthesis of NMOF nanocomposite

In this part, 132 mg of zinc acetate dihydrate was first dissolved in 12.5 mL DMF under vigorous sonication for 10 min at room temperature. Simultaneously, 100 mg 1,4 diazabicyclo[2.2.2]octane and 35 mg terephthalic acid were solubilized in 6.5 mL DMF and followed by strong stirring for 15 min at room temperature. Then, the prepared mixture was added to zinc acetate dehydrate solution under probsonication with 200 W power in pulse mode for 15 min at room temperature. Then the mixture was centrifuged at a speed of 4000 rpm for 12 min, and the precipitant was washed with 10 mL DMF to improve purification quality. Thereafter, 200 mg SDS was solubilized in 12 mL of absolute ethanol and 280 µL of acetic acid.

### 2.5. Ex-situ synthesis of Ag-NMOF

For the ex-situ synthesis of Ag-NMOF (Ge-Ag@NMOF), 10 mL (70 µg/mL) of green synthesized Ag nanoparticle was added into the synthesized NMOF. The mixture was stirred at 60 rpm and left overnight at room temperature, followed by 12 min of centrifugation at 10,000 rpm. The precipitant was dissolved in 10 mL of deionized water, sonicated for 3 h, and kept at a temperature of 4 °C for future use in analytical experiments.

## 2.6. In-situ synthesis of Ag-NMOF

For the in-situ synthesis of Ag-NMOF (Gi-Ag@NMOF), 10 mL of prepared *Spirulina platensis* solution was mixed with 20 mg AgNO<sub>3</sub>, and then the mixture was added to the synthesized NMOF solution. Thereafter, the mixture was stirred at 60 rpm overnight which continued by centrifuging at 10,000 rpm for 12 min and saving the precipitant in 10 mL of deionized water. Also, in the next in-situ synthesis method, 20 mg AgNO<sub>3</sub>, and 10 mL DMF were mixed which followed by adding NMOF solution into the mixture (C-Ag@NMOF). Subsequently, after centrifugation of the prepared mixture at 10,000 rpm for 12 min, the supernatant was removed and the precipitant was saved in 10 mL deionized water.

## 2.7. Preparation of Ag@NMOF-CS-FA nanocomposites

For synthesizing Ag@NMOF-CS-FA nanocomposites, 30 mg CS and 30 mg CS-FA were solubilized in 10 mL of 1 % acetic acid (v/v), and the mixture was stirred at 60 rpm overnight and room temperature to acquire a homogenous solution. Afterward, the prepared mixture was separately solubilized in the previously synthesized Ag@NMOFs with stirring at 50 rpm for 48 h. Consequently, the prepared Ag@NMOF-CS-FA nanocomposites were collected by centrifugation at a speed of 3000 rpm for 15 min and washing with absolute ethanol three times.

## 2.8. Characterization of synthesized nanocomposites

The analysis of nanocomposites involved the use of various analytical devices such as FT-IR, XRD, SERS, DLS, SEM and TEM. The qualification of bond formation and successful endolysin entrapment in chitosan and NMOF was carried out using an FT-IR device. According to standard protocol the wavelength range of 400 cm<sup>-1</sup> to 4000 cm<sup>-1</sup> and the KBr pellet method was used to do this analysis.

The nanocomposites' crystalline state was examined using X-ray diffraction patterns. The test was performed by applying Cu-Ka radiation set at 1.5404 Å on a Bruker D8-advance device equipped with a Lynx Eye detector. The surface of the samples was pressed with a glass slide and the x-ray diffraction patterns were measured at the voltage of 40 kV and current of 30 mA.

SERS device was used to quality the CS-coated Ag@NMOFs and spectra were taken from 100 cm<sup>-1</sup>–4000 cm<sup>-1</sup> on a microscopic confocal Raman spectrometer using a 532 nm He-Ne laser.

Furthermore, the DLS technique was accomplished to reflect the average hydrodynamic diameter of the nanocomposites using the specimens after string sonication by the prob sonication device for a period of 15 min at a temperature of 37 °C. Moreover, measurements of the average hydrodynamic diameter were made at a temperature of 37 °C using samples in a quartz cuvette.

TEM was utilized to examine the morphology, dispersity, and particle size of the Ag@NMOFs nanocomposites. The nanocomposites were spread onto a copper grid and allowed to dry at a temperature of 25 °C before being photographed at the voltage of 120 kV. Excess liquid was removed using filter paper before taking the photographs.

## 2.9. Cell culture

Two distinct cell types, including the human HCT116 colon cancer cell line and human HGF normal cells, were utilized for the purpose of conducting cellular analysis. These cells were each cultured in the RPMI medium, which was supplemented with 10 % FBS, 2 mM glutamine, 100 µg mL<sup>-1</sup> streptomycin, and 100 IU mL<sup>-1</sup> penicillin to ensure optimal growth conditions.

## 2.10. Cell viability assay

The MTT method was used to evaluate cell viability in cancerous and normal cells treated with nanocomposites at varying concentrations (2.5 ng/mL, 5 ng/mL, and 10 ng/mL) for 24 and 48 h. The synthesized samples were initially prepared in a serum-supplemented tissue culture medium and sterilized using 0.2 µm filtration. In what follows, relatively 15000 cells/100 µL of both HCT116 and HGF cells were separately seeded in each well of 96-well microtiter and incubated for 24 h which was followed by replacing old media with fresh media containing different concentrations of synthesized nanocomposites, including NMOF-CS, Ge-Ag@NMOF, Gi-Ag@NMOF, C-Ag@NMOF, Ge-Ag@NMOF-CS-FA, Gi-Ag@NMOF-CS-FA, and C-Ag@NMOF-CS-FA. The cells in the 96-well microtiter were subsequently treated with MTT solution after 24 and 48 h. The final concentration of MTT solution was 0.5 mg/mL per well. Thereafter, the cells were incubated for a period of 4 h at 37 °C in dark conditions before adding the DMSO to dissolve the formed formazan crystals in live cells. Eventually, to measure cell viability, the optical density at 570 nm was read using the ELISA reader device.

## 2.11. Statistical analysis

In this study, the mean ± standard error of the mean was used to express group comparisons and statistical differences in cell viability values were determined using the one-way ANOVA and T-test with significance considered at  $p < 0.05$ .

### 3. Results and discussion

#### 3.1. Characterization of synthesized nano-complexes

##### 3.1.1. FT-IR analysis

The FT-IR approach was used to qualify the synthesized nanocomposites in terms of surface modification and functionalization, and the efficacy of the syntheses, including CS, CS-FA, CS-NMOF, Ge-Ag@NMOF-CS-FA, Gi-Ag@NMOF-CS-FA, and C-Ag@NMOF-CS-FA. Fig. 1 depicts the result of FT-IR analysis.

The major peaks observed in the first graph of pure chitosan include those related to O–H stretching vibration at  $3432\text{ cm}^{-1}$ , symmetric C–H stretching vibration at  $2919\text{ cm}^{-1}$ , asymmetric C–H stretching vibration at  $2871\text{ cm}^{-1}$ , C bending vibration = O at  $1614\text{ cm}^{-1}$ , N–H bending vibration at  $1609\text{ cm}^{-1}$ , CH<sub>2</sub> and CH<sub>3</sub> bending vibration at  $1437\text{ cm}^{-1}$  to  $1393\text{ cm}^{-1}$ , and C–O bending vibration at  $1085\text{ cm}^{-1}$ . The resulting spectrum was compared with standard chitosan, and a correlation was observed [37,38]. To

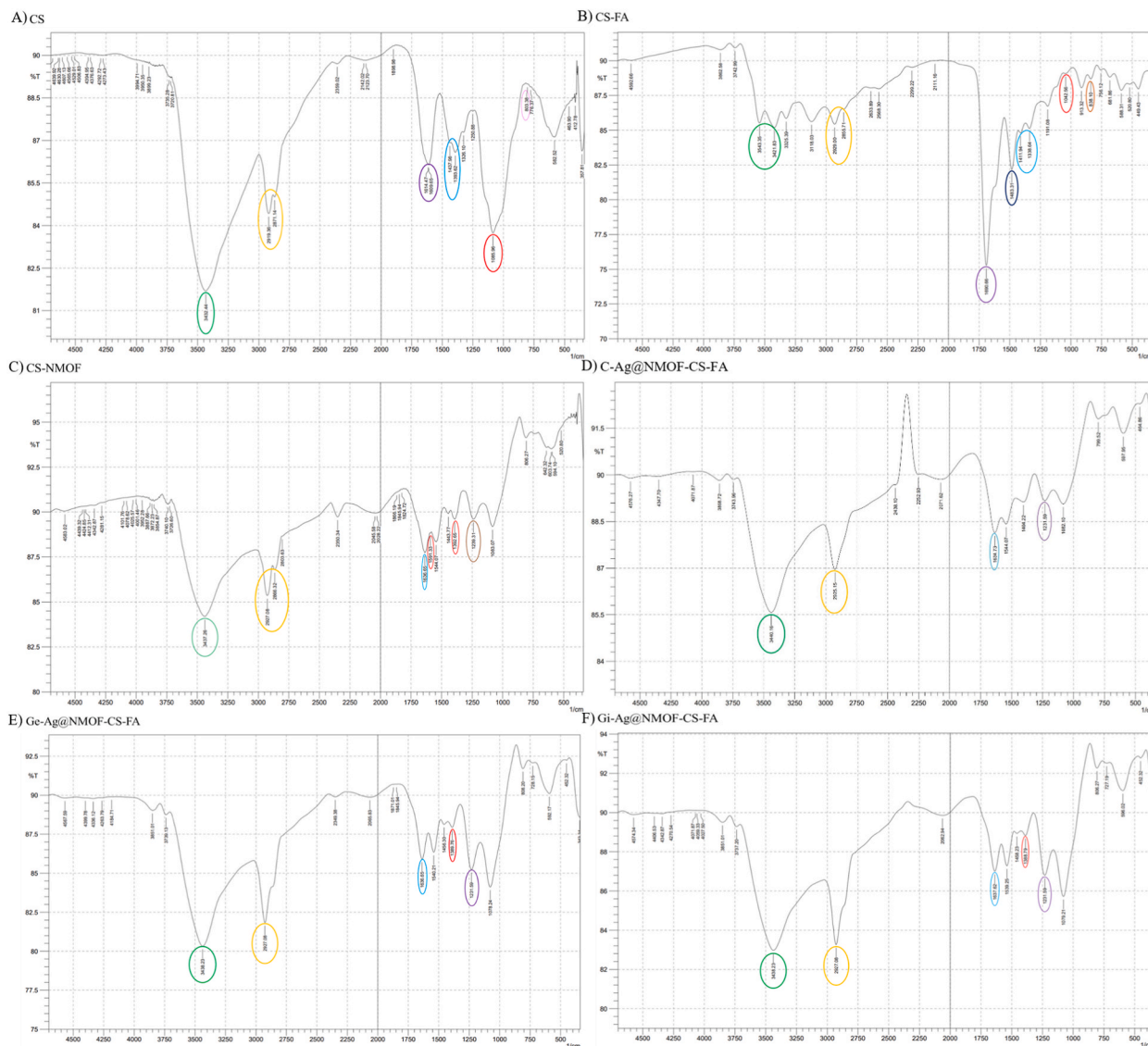


**Fig. 1.** The FT-IR spectra of CS (A), CS-FA (B), CS-NMOF (C), C-Ag@NMOF-CS-FA (D), Ge-Ag@NMOF-CS-FA (E) and Gi-Ag@NMOF-CS-FA (F) specimens. FT-IR analysis revealed significant changes in the peak positions and intensities of different functional groups in these materials. The effective bonding of FA to CS was verified by the distinct peaks associated with chitosan and folic acid functional groups, and a peak related to O–H stretching vibration was detectable within the  $3543\text{ cm}^{-1}$  to  $3421\text{ cm}^{-1}$ . Similarly, the incorporation of silver nanoparticles produced by the green method into MOF cavities caused the COOH group's peak to move to lower wavelength positions in the FTIR diagrams of the produced nanocomposites. These changes in peak positions and intensities serve as evidence of the successful synthesis and functionalization of nanocomposites.

ensure the absence of impurities related to glycosaminoglycans (GAGs), which may be present in impure chitosan, the FT-IR spectrum was thoroughly investigated. The presence of sulphate groups linked to the polysaccharide is confirmed in the FT-IR spectrum by the presence of bands at 1260-1270  $\text{cm}^{-1}$  [39]. However, no signals were observed at 1260-1270  $\text{cm}^{-1}$  in the FTIR diagram of the CS used in this project, indicating the absence of glycosaminoglycan impurity in this sample.

The results of the chitosan-folic acid sample indicate that the conjugation of FA and CS was successful. The FT-IR diagram of this sample revealed noticeable peaks related to functional groups of chitosan and folic acid. The peak corresponding to O-H stretching vibration was observed in the range of 3543  $\text{cm}^{-1}$  to 3421  $\text{cm}^{-1}$ . The peak corresponding to C-H stretching vibration was observed in the range of 2929  $\text{cm}^{-1}$  to 2855  $\text{cm}^{-1}$ . These changes in peak location demonstrate the modifications that occurred after the conjugation reaction of chitosan and folic acid [40]. Furthermore, the C=O bending vibration peak was observed at 1690  $\text{cm}^{-1}$ , the range of the peak corresponding to the C-O-C of the glycosidic bond was observed at 1042  $\text{cm}^{-1}$ , and the peak corresponding to the benzene ring was observed at 838  $\text{cm}^{-1}$ . Additionally, the N-H bending vibration peak observed at 1483  $\text{cm}^{-1}$  is related to the secondary amide group, further supporting the successful conjugation reaction of chitosan and folic acid [41].

The results of the CS-NMOF sample indicate that the hydroxyl group (O-H) peak appears at 3437  $\text{cm}^{-1}$ , while the peaks for CH<sub>2</sub> and CH<sub>3</sub> are between 2927  $\text{cm}^{-1}$  and 2866  $\text{cm}^{-1}$ . In addition, the peak corresponding to aromatic C=C is recorded in the 1636  $\text{cm}^{-1}$ . The symmetric and asymmetric vibrations of carboxyl groups (COOH) in ZnBDC-MOF organic ligands are detected at 1392  $\text{cm}^{-1}$  and 1591  $\text{cm}^{-1}$  [42]. Furthermore, the peak for the C-N bond in NH<sub>2</sub>-BDC can be observed at 1239  $\text{cm}^{-1}$  [43].

In the FT-IR diagram of Ge-Ag@MOF-CS and Gi-Ag@MOF-CS nanocomposites, the peak corresponding to O-H is seen in the range of 3438  $\text{cm}^{-1}$ , while the peaks corresponding to CH<sub>2</sub> and CH<sub>3</sub> are observed at 2927  $\text{cm}^{-1}$ . The peak corresponding to aromatic C=C is recorded at around 1636  $\text{cm}^{-1}$  [27]. The encapsulation of silver nanoparticles synthesized through the green method in MOF pores has caused the peak corresponding to the carboxyl group (COOH) to shift to lower wavenumber positions. In the Ge-Ag@MOF-CS sample, the peak related to the carboxyl group is observed at 1389  $\text{cm}^{-1}$ , and in the Gi-Ag@MOF-CS sample, it is observed at 1388  $\text{cm}^{-1}$ . Due to the synthesis of Ag@MOF nanocomposites, the peak related to the C-O-C is observed at 1231  $\text{cm}^{-1}$  in the FTIR diagram of all three types of synthesized nanocomposites. The most important peak assignments of samples were summarized in Table 1.

### 3.1.2. XRD analysis

X-ray diffraction, a technique in the evaluation of the nanocomposite's structure, was applied for experimenting with the crystallinity and crystallographic orientation of CS-NMOF, Ge-Ag@NMOF-CS-FA, Gi-Ag@NMOF-CS-FA, and C-Ag@NMOF-CS-FA samples [44]. Fig. 2 demonstrates the outputs of this analysis. As shown in Fig. 2, the patterns of XRD have exhibited the crystalline structure of the nanocomposites. The X-ray diffraction patterns of synthesized NMOF nanocomposite confirmed the formation of NMOF and the efficient entrapment of chitosan in NMOF. As the main diffraction peaks at  $2\theta = 17^\circ$ - $43^\circ$ , especially at about  $19.872^\circ$ ,  $27.908^\circ$ , and  $31.532^\circ$ , the crystal structure in the compartment of NMOF while the diffraction peaks of CS are exhibited at around  $2\theta = 6.683^\circ$ - $67.576^\circ$ . The XRD pattern of CS-NMOF nanocomposite indicates visible diffraction peaks at around  $17.278^\circ$ - $27.730^\circ$  that correspond to the diffraction peaks of chitosan [45]. The results of XRD for Ge-Ag@NMOF-CS-FA, Gi-Ag@NMOF-CS-FA, and C-Ag@NMOF-CS-FA samples are as same as that of CS-NMOF, except the disappearance of a peak at  $27.908^\circ$  which could be due to entrapment of Ag nanoparticle in the compartment of CS-NMOF and recrystallization of CS-NMOF. These results effectively approved the formation of the synthesized nanocomposites with a crystalline structure and verified the successful synthesis of Ag-entrapped CS-NMOF.

### 3.1.3. SERS analysis

The preparation of NMOF nanocomposite and its derivatives have also been studied using SERS before and after the conjugation of CS nanoparticles. SERS spectra of eight samples, including the NMOF, CS-NMOF, Ge-Ag@NMOF, Ge-Ag@NMOF-CS, Gi-Ag@NMOF,

**Table 1**

Peak assignment for FTIR spectrum of nanocomposites. This table summarizes characteristic peaks of nanocomposites, such as CS (Chitosan), CS-FA (Chitosan-Folic Acid), CS-NMOF, Ge-Ag@NMOF-CS-FA, Gi-Ag@NMOF-CS-FA, and C-Ag@NMOF-CS-FA. Due to the synthesis of Ag@MOF nanocomposites, the peak related to the C-O-C stretching is observed at 1231  $\text{cm}^{-1}$  in the FTIR diagram of all Ag@MOF nanocomposites. Moreover, the effective bonding of folic acid to chitosan is verified.

Assignments	Wavelength ( $\text{cm}^{-1}$ )			
	CS (Chitosan)		CS-FA (Chitosan-Folic Acid)	
O-H Stretching	3432		3543-3421	
C-H Stretching	2919-2871		2929-2855	
C=O Bending	1614		1690	
N-H Bending	1609		1483	
CH <sub>2</sub> /CH <sub>3</sub> Bending	1437-1393		1411-1338	
C-O Bending	1085		1042	
Assignments	CS-NMOF	Ge-Ag@NMOF-CS	Gi-Ag@NMOF-CS	C-Ag@NMOF-CS
O-H Stretching	3437	3438	3438	3440
C=C Bending	1636	1636	1637	1634
CH <sub>2</sub> /CH <sub>3</sub> Bending	2927-2866	2927	2927	2925
Carboxyl group	1392-1591	1389	1388	1404
C-O-C Stretching	1239	1231	1231	1231

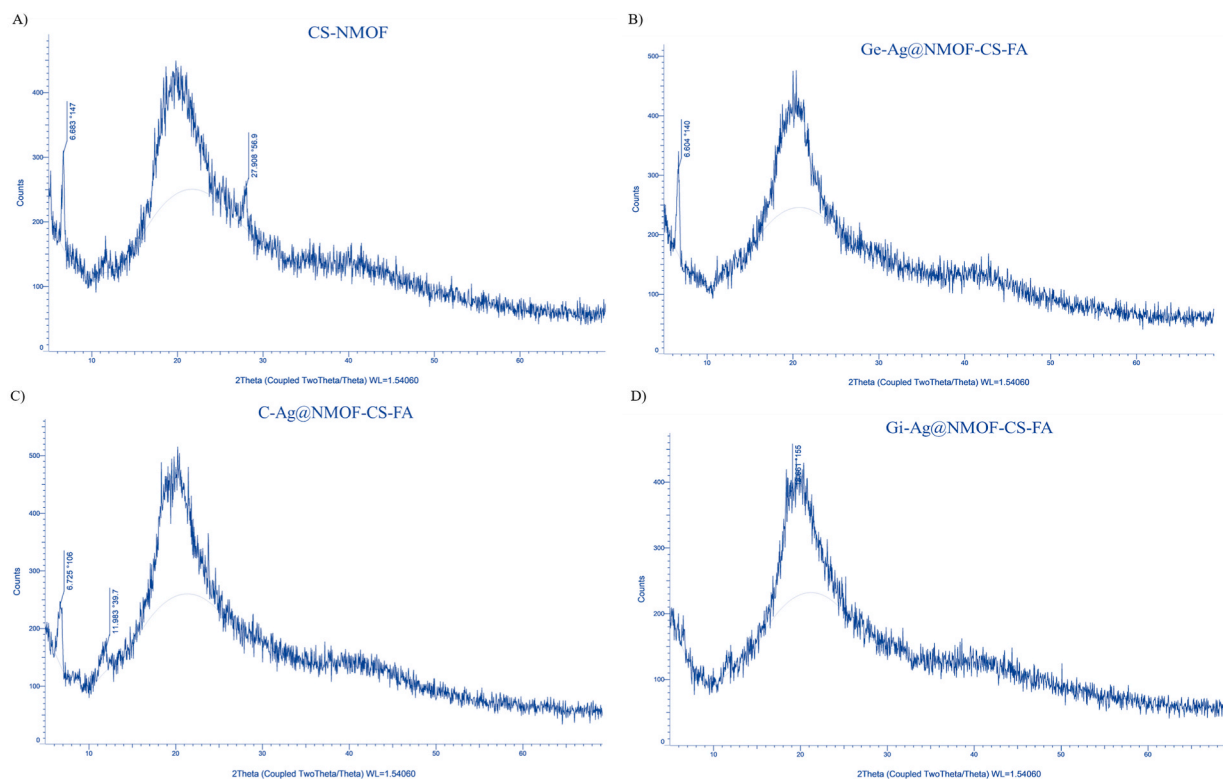


**Fig. 2.** The powder XRD patterns of CS-NMOF (A), Ge-Ag@NMOF-CS-FA (B), C-Ag@NMOF-CS-FA (C), and Gi-Ag@NMOF-CS-FA (D) samples. The XRD data for Ge-Ag@NMOF-CS-FA, C-Ag@NMOF-CS-FA, and Gi-Ag@NMOF-CS-FA samples are as same as that of CS-NMOF, except the disappearance of a peak at  $27.908^\circ$  which could be due to entrapment of Ag nanoparticle in the compartment of CS-NMOF and recrystallization of CS-NMOF.

Gi-Ag@NMOF-CS, C-Ag@NMOF, and C-Ag@NMOF-CS-FA nanocomposites, are indicated in Fig. 3. SERS is a practical method for ascertaining the authenticity of carbon-based composites [46]. The peaks related to the stretching of  $sp^3$  and  $sp^2$  carbon could be detected in the SERS of carbon materials [47]. The SERS peaks of the NMOF are found at around  $1423\text{ cm}^{-1}$ ,  $1609\text{ cm}^{-1}$ ,  $1135\text{ cm}^{-1}$ , and  $863\text{ cm}^{-1}$  which assigns the vibrational mode of a 1,4-benzene dicarboxylic acid; to put in more vivid epicure, the peaks at  $1504\text{ cm}^{-1}$ ,  $1356\text{ cm}^{-1}$ ,  $1311\text{ cm}^{-1}$ , and  $1186\text{ cm}^{-1}$  are assigned to the C-H in-plane bending, C-O-C stretching and C-C stretching of the aromatic ring, respectively [41]. According to the graphs, after coating Ag@NMOF with CS nanoparticles, the Raman intensity of samples is considerably increased in all samples; for instance, after CS coating in NMOF, the Raman intensity is enhanced from 1200 a. u. to 8000 a.u. while this figure is extensively higher for Ge-Ag@NMOF samples after entrapment with CS, 1500 a.u. to 200,000 a.u., the same results are attained for Gi-Ag@NMOF (from 4000 a.u. to 200,000 a.u.) and C-Ag@NMOF (from 2000 a.u. to 3000 a.u.) nanocomposites as well. The recorded enhancement in the signals could be owing to the rough perforated surface of Ag-decorated NMOF nanocomposites after CS coating that, in turn, can contribute to the rising in interparticle nanogaps and subsequently result in high-density hot spots [48].

### 3.1.4. Size and morphology analyses

The DLS, TEM, and SEM devices were used to investigate the size, distribution, and morphology of nanocomposites. Fig. 4 presents the outputs of these analyses. DLS technique, as a kind of spectroscopy, is an appropriate approach for scrutinizing the hydrodynamic diameter and polydispersity index (PDI) nano-size samples. As can be seen from Fig. 4, the hydrodynamic diameters of NMOF-CS, Ge-Ag@NMOF-CS, Gi-Ag@NMOF-CS, and C-Ag@NMOF-CS specimens were measured at around 99.7 nm, 150 nm, 128 nm, 150 nm, respectively that are in the range of nanometric size and suitable for delivery of theranostics. The nanometric size of particles is very important in the successful drug delivery to the cancerous tissues, and chemo-physical serum stability, getting away from the immune system, and efficient uptake in cancer cells are either directly or indirectly relevant to the size of nano-devices in nano delivery systems [49]. Besides, the PDI values of these nanocomposites were determined about 0.14, 0.17, 0.2, 0.19 for NMOF-CS, Ge-Ag@NMOF-CS, Gi-Ag@NMOF-CS, and C-Ag@NMOF-CS nanocomposites, respectively which confirms the reliable distribution of nanocarriers since PDIs less than 0.2 are said to be suitable for great dispersity, appropriate serum stability, good therapeutic efficiency, and minimizing the aggregation and agglomeration of nanocomposites [50].

Furthermore, in order to exact size investigation of the synthesized nanocomposites, the TEM method was conducted. The TEM image of Gi-Ag@NMOF-CS, Ge-Ag@NMOF-CS and C-Ag@NMOF-CS nanocomposites were taken and its results (Fig. 4B) revealed

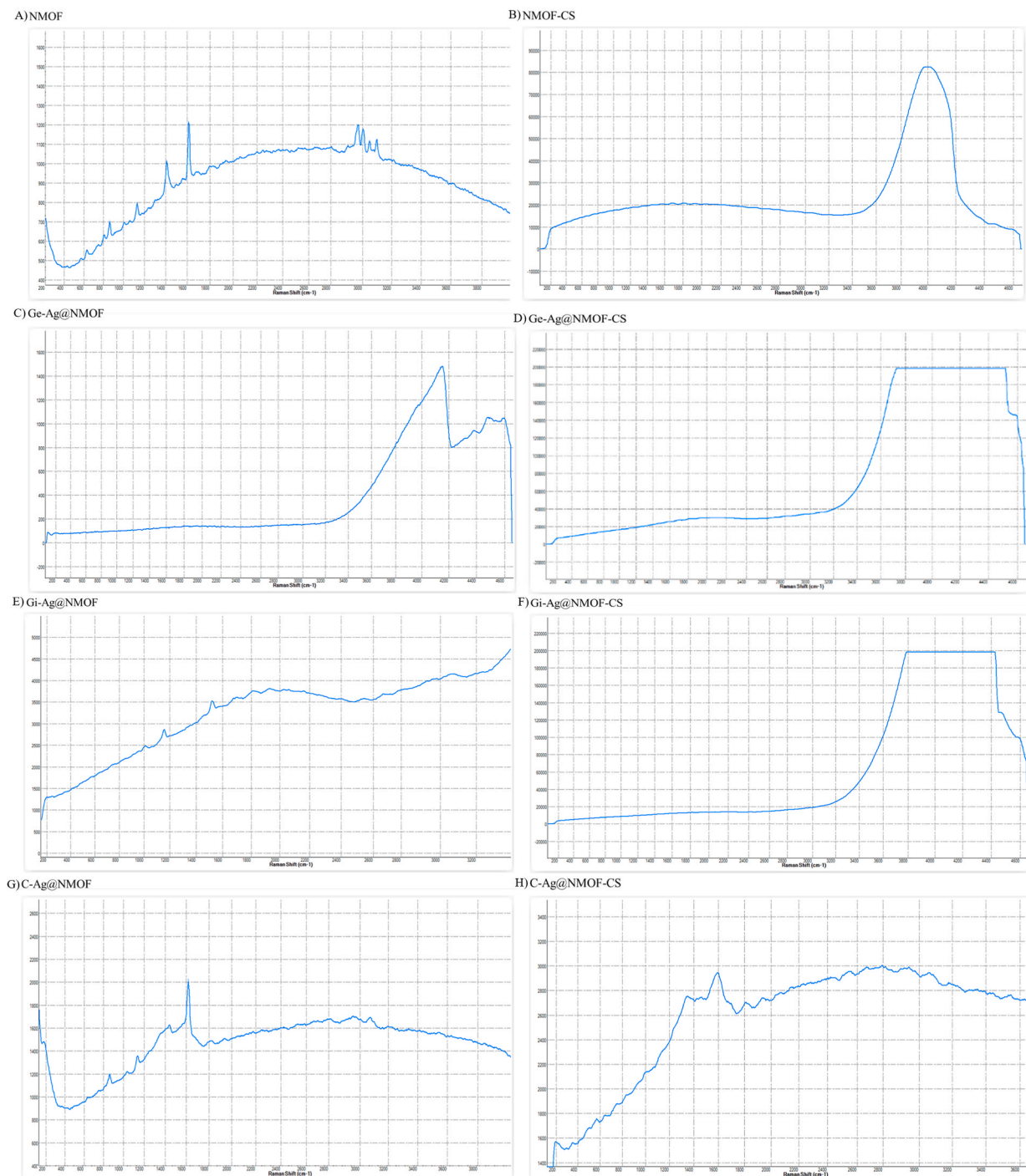
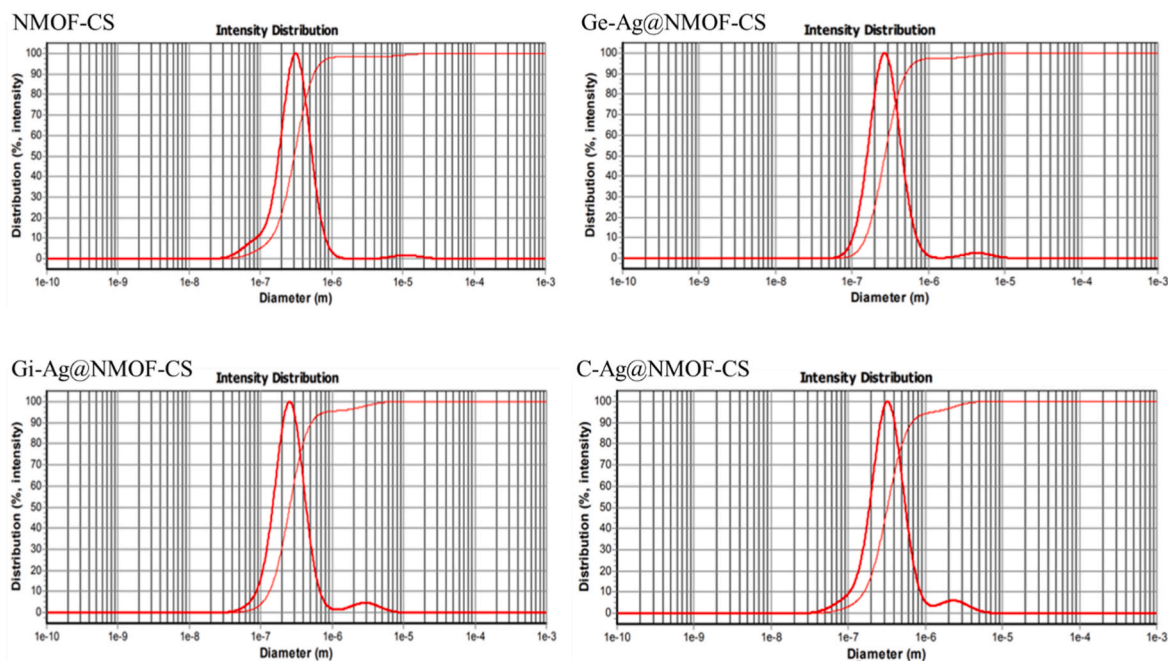


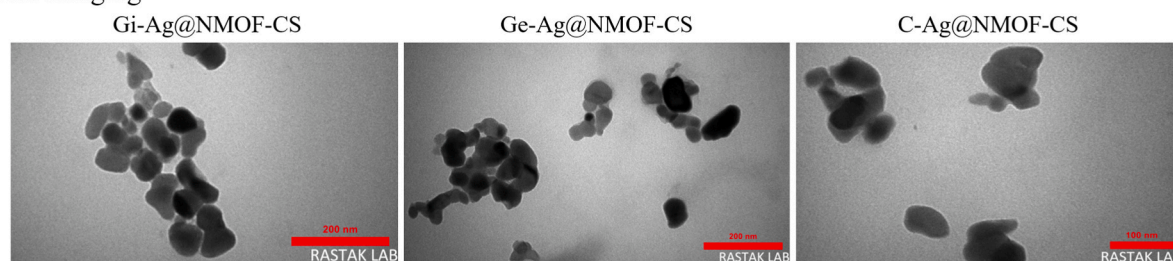
**Fig. 3.** The SERS spectra of NMOF (A), CS-NMOF (B), Ge-Ag@NMOF (C), Ge-Ag@NMOF-CS (D), Gi-Ag@NMOF (E), Gi-Ag@NMOF-CS (F), C-Ag@NMOF (G), and C-Ag@NMOF-CS (H) nanocomposites. The SERS peaks of the NMOF are found at  $1423\text{ cm}^{-1}$ ,  $1609\text{ cm}^{-1}$ ,  $1135\text{ cm}^{-1}$ , and  $863\text{ cm}^{-1}$  that are corresponded to the vibrational mode of a 1,4-benzene dicarboxylic acid. Also, the Raman intensity of the samples improved significantly in all cases when CS was used to coat Ag@NMOF.

nearly a narrow particle size distribution with an average size smaller than 100 nm in diameter. There are porous structures and a gelatinous layer on the surface of the picture of the TEM image of Gi-Ag@NMOF-CS nanocomposite (Fig. 4, left TEM image) which are indicators of the NMOF network and chitosan on the surface of the nanocomposite, respectively. A diameter smaller than 200 nm is considered ideal for delivering drugs to cancerous tissues, as it allows for effective distribution in cancer tissue capillaries and

## A) DLS Analysis



## B) TEM Imaging



## C) SEM Imaging

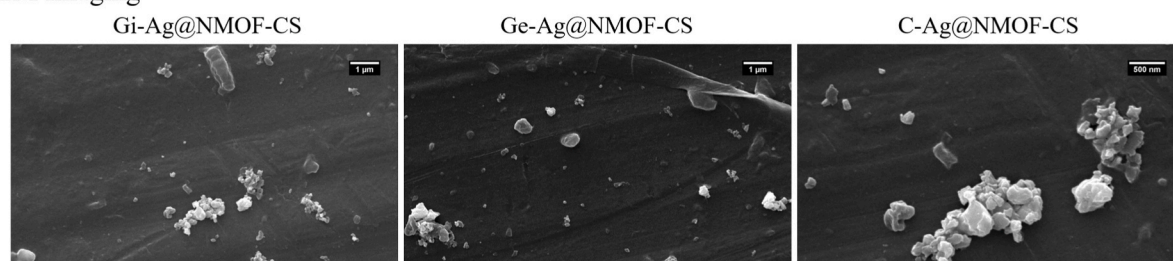


**Fig. 4.** DLS analysis of NMOF-CS, Ge-Ag@NMOF-CS, Gi-Ag@NMOF-CS, and C-Ag@NMOF-CS nanocomposites, and TEM and SEM images of Gi-Ag@NMOF-CS, Ge-Ag@NMOF-CS and C-Ag@NMOF-CS samples. The size of NMOF nanocomposites was measured to be between 100 nm and 160 nm through DLS analysis, and their dispersity was appropriate. TEM images have indicated that the particle size distribution is narrow, with an average diameter of less than 100 nm for all samples. SEM images have presented the size range as same as that of the DLS technique, and the semispherical morphology has been determined for nanocomposites according to SEM images as well.

subsequently facilitates the internalization of nanocarriers into cancer cells [51]. Also, good blood circulation and a high level of internalization into cancer cells through enhanced permeability and retention (EPR) effect are other characteristics of nano-delivery systems in cancer therapy [52]. On the other hand, the SEM results of Gi-Ag@NMOF-CS, Ge-Ag@NMOF-CS and C-Ag@NMOF-CS nanocomposites (Fig. 4C) were taken and the data demonstrated even distribution and approximately semi-globular shape and morphology. These semispherical shapes could be due to the porous structure of NMOF and its modified surface with CS nanoparticles and even using lyophilized samples for SEM tests. The size was determined between the range of 100 nm–200 nm using an SEM device

which is in line with the outputs of DLS and TEM.

### 3.2. Cell viability assay

The toxicity of various nanocomposites, such as NMOF, CS-NMOF, NMOF-CS-FA, Ge-Ag@NMOF, Ge-Ag@NMOF-CS-FA, Gi-Ag@NMOF, Gi-Ag@NMOF-CS-FA, C-Ag@NMOF, and C-Ag@NMOF-CS-FA, was evaluated through a biocompatibility and cancer cell suppression study using MTT assay (Fig. 5). The study examined the effects of time and concentration of nanocomposites on the survival of normal and colon cancer cells after treatment with 2.5 ng/mL (C3), 5 ng/mL (C2), and 10 ng/mL (C1) concentrations for 24 h and 48 h.

Results from Fig. 5 indicated that FA-functionalized nanocomposites performed better in inhibiting cancer cells than other samples. Treatment time of 24 h showed better cytotoxicity performance for colon cancer cells with FA-decorated samples (except for 10 ng/mL), while the reverse was true for normal cells (Fig. 5 A and C). The viability of cancer cells treated with all concentrations of nanocomposites without FA was lower after 48 h compared to 24 h, further confirming the impact of FA in targeting cancer cells (Fig. 5 B and D).

The Ge-Ag@NMOF-CS-FA sample showed better cytotoxicity on colon cancer cells, with about 38 % cell viability after 24 h of treatment with 10 ng/mL concentration compared to other nanocomposites with FA, which stood at around 50 %. Thus, The IC50 value for colon cancer cells was obtained at 24 h by Ge-Ag@NMOF-CS-FA at 10 ng/mL concentration (Fig. 5C). The IC50 values of HCT116 cells, after 48 h of treatment with NMOF-CS-FA, Ge-Ag@NMOF-CS-FA, Gi-Ag@NMOF-CS-FA, and C-Ag@NMOF-CS-FA samples, were attained for 10 ng/mL concentration (Fig. 5D).

Samples containing Ag nanoparticles did not show any significant difference in cell viability values compared to those without Ag, indicating the non-toxic effects of Ag nanoparticles on cancer cells. The higher internalization of FA-decorated nanocomposites induced toxicity in cancer cells by accumulating nanocomposites inside.

Cancer cell viability after treatment with nanocomposites without FA ranged from 80 % to 93 % for both treatment times. However,

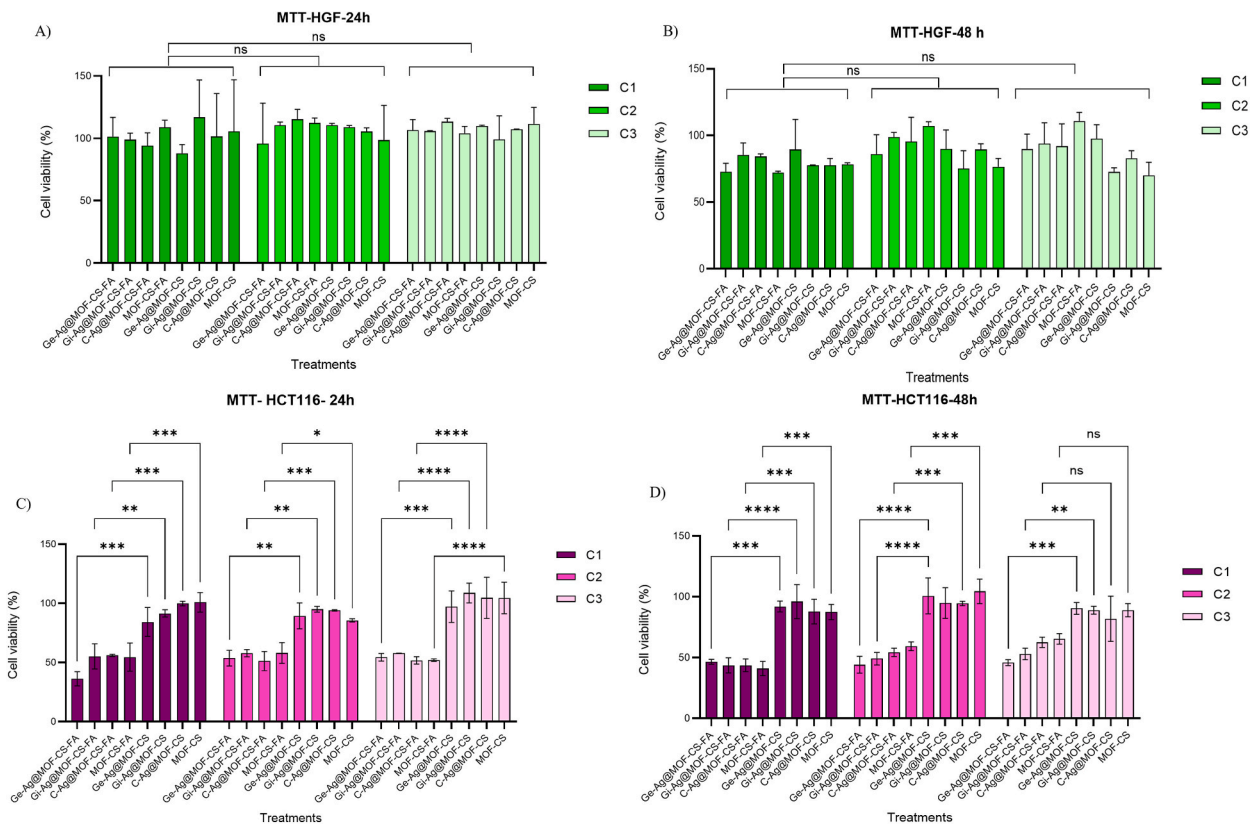


**Fig. 5.** The cytotoxic effects of various nanocomposites, including NMOF, CS-NMOF, NMOF-CS-FA, Ge-Ag@NMOF, Ge-Ag@NMOF-CS-FA, Gi-Ag@NMOF, Gi-Ag@NMOF-CS-FA, C-Ag@NMOF, and C-Ag@NMOF-CS-FA, on HGF normal (A and B) and HCT116 colon cancer cells (C and D) at 2.5 ng/mL (C3), 5 ng/mL (C2), and 10 ng/mL (C1) concentrations for 24 and 48 h. Good biocompatibility was obtained for the NMOF nanocomposite and its derivatives. FA functionalized nanocomposites performed better in inhibiting cancer cells than other samples, while the effects of concentrations are not as much as the effects of kinds of samples. The IC50 value for colon cancer cells was obtained at 24 h by Ge-Ag@NMOF-CS-FA at 10 ng/mL concentration. The IC50 values of HCT116 cells, after 48 h of treatment with NMOF-CS-FA, Ge-Ag@NMOF-CS-FA, Gi-Ag@NMOF-CS-FA, and C-Ag@NMOF-CS-FA samples, were attained for 10 ng/mL concentration.

for HGF normal cells, there was no less than 85 % cell viability after treatment with various concentrations of nanocomposites at 24 h of post-treatment, indicating that there is no considerable amount of FA receptors on the surface of normal cells (Fig. 5 A). This result shows that synthesized nanocomposites can be used for the treatment of cancer in the human body with very low toxic effects on normal cells. In comparison to the Zhang et al. [53] research, in which a miRNA-Guided Zn-NMOF-based nanocarrier was developed for imaging and photodynamic treatment of breast cancer cells, our findings are in accordance with their results in the biocompatibility of NMOF and its performance in targeting MCF-10A, MDA-MB-231, and OVAR-3 cancer cells. More than 90 % cell viability was acquired for their NMOF in cancer cells after 24 h of treatment with various types of NMOFs at nM concentrations.

#### 4. Conclusion

In this project, a novel nano-delivery system was successfully created to suppress colon cancer cells. The impact of different synthesis approaches, including ex-situ and in-situ methods, on the physical and chemical properties of Ag@MOF nanocomposites were examined; Silver nanoparticles were attached to a metal-organic framework (MOF) to synthesize Ag@MOF nanocomposites. The synthesized nanocomposites, Ge-Ag@MOF, Gi-Ag@MOF, and C-Ag@MOF-CS, were coated by using chitosan polymer and targeted with folic acid. Various analytical devices such as FT-IR, DLS, SERS, SEM, and TEM were applied to the characterization of nanocomposites. The results showed that the in-situ method was more efficient and appropriate in synthesizing silver nanoparticles inside the MOF structure, which created optimal hot spots within the metal-organic frameworks. However, controlling the size of the synthesized nanoparticles inside the MOFs was challenging when using the in-situ method. The ex-situ method was able to produce nanocomposites of a more suitable size and fewer peaks. Subsequently, the cell viability experiment was used to investigate the effectiveness of targeted nanocomposites in suppressing the growth of colon cancer cells. The results showed that the FA-targeted Ag@NMOF-CS nanocomposite was efficient in both internalization and inhibition of cancer cell growth.

#### Ethical approval

Ethical code. IR.IAU.PS.REC.1400.321.

#### Consent to participate

The authors declare that they have consent to participate.

#### Consent to publish

The authors declare that they have consent to publish.

#### Complete ethics statement

The authors declare that they have no known competing financial interests or personal relationships that could have appeared to influence the work reported in this paper.

#### Data availability statement

Availability of data and materials: The data that support the findings of this study are available on request from the corresponding author. Data associated with this study has not been deposited into a publicly available repository.

#### CRedit authorship contribution statement

**Fatemeh Mahboubi:** Project administration, Methodology, Investigation. **Javad Mohammadnejad:** Data curation, Conceptualization. **Sepideh Khaleghi:** Writing – review & editing, Visualization, Validation, Supervision, Software, Resources, Project administration, Methodology, Investigation, Formal analysis, Data curation, Conceptualization.

#### Declaration of competing interest

The authors declare that they have no known competing financial interests or personal relationships that could have appeared to influence the work reported in this paper.

#### References

- [1] F.N. Golafzani, et al., Delivery of miRNA-126 through folic acid-targeted biocompatible polymeric nanoparticles for effective lung cancer therapy, *J. Bioact. Compat Polym.* 37 (3) (2022) 168–188.
- [2] D. Ion, et al., An up-to-date review of natural nanoparticles for cancer management, *Pharmaceutics* 14 (2022) 18, 2021, s Note: MDPI stays neutral with regard to jurisdictional claims in.

- [3] P. Rawla, T. Sunkara, A. Barsouk, Epidemiology of colorectal cancer: incidence, mortality, survival, and risk factors, *Gastroenterology Review/Przegląd Gastroenterologiczny* 14 (2) (2019) 89–103.
- [4] S. Ding, et al., Overcoming blood-brain barrier transport: advances in nanoparticle-based drug delivery strategies, *Mater. Today* 37 (2020) 112–125.
- [5] J. Wang, et al., Bioorthogonal SERS nanotags as a precision theranostic platform for in vivo SERS imaging and cancer photothermal therapy, *Bioconjugate Chem.* 31 (2) (2020) 182–193.
- [6] S. Wen, et al., Aptamer-conjugated Au Nanocage/SiO<sub>2</sub> core-shell bifunctional nanoprobe with high stability and biocompatibility for cellular SERS imaging and near-infrared photothermal therapy, *ACS Sens.* 4 (2) (2019) 301–308.
- [7] M.M. Joseph, et al., Exploring the margins of SERS in practical domain: an emerging diagnostic modality for modern biomedical applications, *Biomaterials* 181 (2018) 140–181.
- [8] Y. Zhang, et al., Ultrabright gap-enhanced Raman tags for high-speed bioimaging, *Nat. Commun.* 10 (1) (2019) 3905.
- [9] A. Baeza, D. Ruiz-Molina, M. Vallet-Regí, Recent advances in porous nanoparticles for drug delivery in antitumoral applications: inorganic nanoparticles and nanoscale metal-organic frameworks, *Expert Opin. Drug Deliv.* 14 (6) (2017) 783–796.
- [10] A. Narmani, et al., Gadolinium nanoparticles as diagnostic and therapeutic agents: their delivery systems in magnetic resonance imaging and neutron capture therapy, *J. Drug Deliv. Sci. Technol.* 44 (2018) 457–466.
- [11] M. Akhlaq, et al., Methotrexate-loaded gelatin and polyvinyl alcohol (Gel/PVA) hydrogel as a pH-sensitive matrix, *Polymers* 13 (14) (2021) 2300.
- [12] A. Narmani, K. Yavari, J. Mohammadnejad, Imaging, biodistribution and in vitro study of smart 99mTc-PAMAM G4 dendrimer as novel nano-complex, *Colloids Surf. B Biointerfaces* 159 (2017) 232–240.
- [13] Y. Wang, et al., Hierarchical micro/nanofibrous scaffolds incorporated with curcumin and zinc ion eutectic metal organic frameworks for enhanced diabetic wound healing via anti-oxidant and anti-inflammatory activities, *Chem. Eng. J.* 402 (2020) 126273.
- [14] D. Han, et al., Phototherapy-strengthened photocatalytic activity of polydopamine-modified metal-organic frameworks for rapid therapy of bacteria-infected wounds, *J. Mater. Sci. Technol.* 62 (2021) 83–95.
- [15] E. Naderlou, et al., Enhanced sensitivity and efficiency of detection of *Staphylococcus aureus* based on modified magnetic nanoparticles by photometric systems, *Artif. Cell Nanomed. Biotechnol.* 48 (1) (2020) 810–817.
- [16] S. Khaleghi, et al., The effect of superparamagnetic iron oxide nanoparticles surface engineering on relaxivity of magnetoliposome, *Contrast Media Mol. Imaging* 11 (5) (2016) 340–349.
- [17] T. Sun, et al., Hydrophobicity-adjustable MOF constructs superhydrophobic MOF-rGO aerogel for efficient oil-water separation, *ACS Appl. Mater. Interfaces* 12 (50) (2020) 56435–56444.
- [18] B.E. El Bialy, et al., Cytotoxic effect of biosynthesized silver nanoparticles on Ehrlich ascites tumor cells in mice, *Int. J. Pharmacol.* 13 (2) (2017) 134–144.
- [19] A. Alahmad, et al., Hypericum perforatum L.-mediated green synthesis of silver nanoparticles exhibiting antioxidant and anticancer activities, *Nanomaterials* 11 (2) (2021) 487.
- [20] P. Roychoudhury, et al., Cyanobacteria assisted biosynthesis of silver nanoparticles—a potential antileukemic agent, *J. Appl. Phycol.* 28 (2016) 3387–3394.
- [21] M. Skiba, et al., Green synthesis of nanoparticles of precious metals: antimicrobial and catalytic properties, *Восточно-Европейский Журнал передовых технологий* 5 (6) (2018) 51–58.
- [22] G. Sharma, et al., Biological synthesis of silver nanoparticles by cell-free extract of *Spirulina platensis*, *Journal of nanotechnology* 2015 (2015) 1–6.
- [23] F. Ameen, et al., Fabrication of silver nanoparticles employing the cyanobacterium *Spirulina platensis* and its bactericidal effect against opportunistic nosocomial pathogens of the respiratory tract, *J. Mol. Struct.* 1217 (2020) 128392.
- [24] A. Sidorowicz, et al., Characterization of nanomaterials synthesized from *Spirulina platensis* extract and their potential antifungal activity, *PLoS One* 17 (9) (2022) e0274753.
- [25] O. Pivovarov, et al., Preparation of silver nanoparticles by contact nonequilibrium low-temperature plasma in the presence of sodium alginate, *Вопросы химии и химической технологии* (6) (2017) 82–88.
- [26] M. Skiba, et al., Plasmochemical preparation of silver nanoparticles: thermodynamics and kinetics analysis of the process, *Восточно-Европейский Журнал передовых технологий* 2 (6) (2018) 4–9.
- [27] A.H. Al-Badwy, et al., Polysaccharides from *Spirulina platensis* (PSP): promising biostimulants for the green synthesis of silver nanoparticles and their potential application in the treatment of cancer tumors, *Microb. Cell Factories* 22 (1) (2023) 247.
- [28] M. Rezvani, et al., Synthesis and in vitro study of modified chitosan-polycaprolactam nanocomplex as delivery system, *Int. J. Biol. Macromol.* 113 (2018) 1287–1293.
- [29] D. Wu, et al., Chitosan-based colloidal polyelectrolyte complexes for drug delivery: a review, *Carbohydr. Polym.* 238 (2020) 116126.
- [30] A. Zamanvaziri, et al., Targeted PEGylated chitosan nano-complex for delivery of sodium butyrate to prostate cancer: an in vitro study, *Technol. Cancer Res. Treat.* 22 (2023) 15330338231159223.
- [31] K. Mortezaee, et al., Synergic effects of nanoparticles-mediated hyperthermia in radiotherapy/chemotherapy of cancer, *Life Sci.* 269 (2021) 119020.
- [32] A. Narmani, et al., Folic acid functionalized nanoparticles as pharmaceutical carriers in drug delivery systems, *Drug Dev. Res.* 80 (4) (2019) 404–424.
- [33] N. Mokri, et al., Chitosan-coated Zn-metal-organic framework nanocomposites for effective targeted delivery of LNA-antisense miR-224 to colon tumor: in vitro studies, *Gene Ther.* 29 (12) (2022) 680–690.
- [34] A. Narmani, et al., Breast tumor targeting with PAMAM-PEG-5FU-99m Tc as a new therapeutic nanocomplex: in in-vitro and in-vivo studies, *Biomed. Microdevices* 22 (2020) 1–13.
- [35] A. Narmani, J. Mohammadnejad, K. Yavari, Synthesis and evaluation of polyethylene glycol-and folic acid-conjugated polyamidoamine G4 dendrimer as nanocarrier, *J. Drug Deliv. Sci. Technol.* 50 (2019) 278–286.
- [36] I. Barwal, et al., Targeted delivery system for cancer cells consist of multiple ligands conjugated genetically modified CCMV capsid on doxorubicin GNPs complex, *Sci. Rep.* 6 (1) (2016) 37096.
- [37] R. Varma, S. Vasudevan, Extraction, characterization, and antimicrobial activity of chitosan from horse mussel *modiolus modiolus*, *ACS Omega* 5 (32) (2020) 20224–20230.
- [38] A.A. Moosa, A.M. Ridha, N.A. Kadhim, Use of biocomposite adsorbents for the removal of methylene blue dye from aqueous solution, *Am. J. Mater. Sci.* 6 (5) (2016) 135–146.
- [39] M.F. Queiroz, et al., Does the use of chitosan contribute to oxalate kidney stone formation? *Mar. Drugs* 13 (1) (2014) 141–158.
- [40] S. Bandara, et al., Synthesis and characterization of Zinc/Chitosan-Folic acid complex, *Heliyon* 4 (8) (2018) e00737.
- [41] M.K. Viswanadh, et al., Bioadhesive chitosan nanoparticles: dual targeting and pharmacokinetic aspects for advanced lung cancer treatment, *Carbohydr. Polym.* 274 (2021) 118617.
- [42] R. Dutta, M.N. Rao, A. Kumar, Investigation of ionic liquid interaction with ZnBDC-metal organic framework through scanning EXAFS and inelastic neutron scattering, *Sci. Rep.* 9 (1) (2019) 14741.
- [43] R. Sacourbaravi, et al., Fabrication of Ag NPs/Zn-MOF nanocomposites and their application as antibacterial agents, *J. Inorg. Organomet. Polym. Mater.* 30 (2020) 4615–4621.
- [44] X. Jia, et al., Immobilization of chitosan grafted carboxylic Zr-MOF to porous starch for sulfanilamide adsorption, *Carbohydr. Polym.* 253 (2021) 117305.
- [45] M.E.A. Ali, et al., Chitosan nanoparticles extracted from shrimp shells, application for removal of Fe (II) and Mn (II) from aqueous phases, *Separ. Sci. Technol.* 53 (18) (2018) 2870–2881.
- [46] P. Wang, et al., One-step synthesis of easy-recycling TiO<sub>2</sub>-rGO nanocomposite photocatalysts with enhanced photocatalytic activity, *Appl. Catal. B Environ.* 132 (2013) 452–459.
- [47] Z. Gharehdaghi, et al., Cu (II)-porphyrin metal-organic framework/graphene oxide: synthesis, characterization, and application as a pH-responsive drug carrier for breast cancer treatment, *J. Biol. Inorg. Chem.* 26 (2021) 689–704.

- [48] C. Puente, et al., Silver-chitosan and gold-chitosan substrates for surface-enhanced Raman spectroscopy (SERS): effect of nanoparticle morphology on SERS performance, *Mater. Chem. Phys.* 260 (2021) 124107.
- [49] W. Tan, et al., Novel cationic chitosan derivative bearing 1, 2, 3-triazolium and pyridinium: synthesis, characterization, and antifungal property, *Carbohydr. Polym.* 182 (2018) 180–187.
- [50] N. Faramarzi, et al., Synthesis and in vitro evaluation of tamoxifen-loaded gelatin as effective nanocomplex in drug delivery systems, *Int. J. Nanosci.* 19 (5) (2020) 2050002.
- [51] V.R. Kanth, et al., Blend hydrogel microspheres of carboxymethyl chitosan and gelatin for the controlled release of 5-fluorouracil, *Pharmaceutics* 9 (2) (2017) 13.
- [52] Y. Li, et al., Dynamic light scattering immunosensor based on metal-organic framework mediated gold growth strategy for the ultra-sensitive detection of alpha-fetoprotein, *Sensor. Actuator. B Chem.* 341 (2021) 130030.
- [53] P. Zhang, et al., miRNA-guided imaging and photodynamic therapy treatment of cancer cells using Zn (II)-protoporphyrin IX-loaded metal-organic framework nanoparticles, *ACS Nano* 16 (2) (2022) 1791–1801.